The 8th European Congress on Computational Methods in Applied Sciences and Engineering
ECCOMAS Congress 2022
5 – 9 June 2022, Oslo, Norway

COMPUTATIONAL MODELLING AND CHARACTERIZATION OF NON-NEWTONIAN VISCO-PLASTIC CEMENTITIOUS BUILDING MATERIALS

Mareike Thiedeitz[*], Jithender J. Timothy[†] and Thomas Kränkel[†]

Technical University Munich, centre for building materials,

[*] mareike.thiedeitz@tum.de, [†] jithender.timothy@tum.de, [†] thomas.kraenkel@tum.de

Key words: *non-Newtonian flow, cement paste, computational fluid dynamics, visco-plastic modelling, concrete rheology*

Abstract. Cementitious building materials like Ultra High Performance Concrete (UHPC), Self-Compacting Concrete (SCC) or concrete with low clinker content possess complex rheological properties. Due to high packing densities and the use of various additives and chemical admixtures, a huge range of non-Newtonian flow characteristics from shear-thinning to shear-thickening, visco-elastic material behaviour and structural build-up can appear. For these concretes, transient computational modelling using Computational Fluid Dynamics (CFD) requires a meaningful choice of rheological parameters and the associated boundary conditions. The authors present the rheological analysis of five cementitious pastes with low (ϕ = 0.45) to high (ϕ = 0.58) solid volume fraction ϕ. Rheological parameters from rheometric flow protocols are compared with empirical stoppage test results for short and steady (slump flow) and transient flow (L-Box) conditions. Following, numerical simulation with the measured rheological parameters as input parameters is compared to the experimental flow results. CFD analysis using OpenFOAM is performed for the flow in empirical stoppage tests. We found that with increasing non-Newtonian behaviour, deviations between real and simulated flow appear due to insufficient transient flow descriptions and unknown secondary effects. The results provide new insight into computational modelling of complex cementitious building materials and serve as basis for further advanced CFD based modelling and characterization of time-dependent non-Newtonian concrete flow.

1 INTRODUCTION

Computational modelling of concrete casting is a suitable tool to predict processing and casting properties of fresh concrete, analyse and adjust necessary flowability properties and thus enhance the final structural element quality [1]. Cementitious building materials and concrete are heterogeneous suspensions with size scales of interest ranging from several µm (colloidal particles within the cementitious paste) and cm (aggregates) to m (casting behaviour in formworks). Computational Fluid Dynamics (CFD) considers concrete as homogeneous continuum. The constitutive governing equations are based on Newtonian flow and use the Navier-Stokes equations [2]. For yield stress fluids, e.g. the Bingham – or the Herschel-Bulkley model are implemented into the material-dependent stress tensor [3, 4]; and more advanced modelling approaches also take thixotropic behaviour into account [5–7]. State-of-the-art standardized empirical stoppage tests (slump flow test acc. [8] and L-Box test acc. [9]) correlate flow tests to rheological (i.e. Bingham) parameters. This research presents the comparison

between empirical stoppage tests, rheometric analysis and flow simulations of cementitious pastes over different time scales in dependence of their rheological properties.

1.1 Rheology of non-Newtonian cementitious pastes

Cementitious pastes are two-phase colloidal suspensions with solid particles ranging from several nm to 100 µm and dispersed in an ionic pore solution. Below a certain particle distance, particle interaction forces (both attractive and repulsive depending on the chemical composition and physical granulometric properties, [10, 11]) take place and affect the rheological flow behavior. The water to binder ratio (w/b ratio) of the paste determines the solid volume fraction ϕ_s and thus particle distances. ϕ_s is calculated as the ratio between the volume of solids and the total volume ($\phi_s = {}^{V_s}/_{V_t}$). In dilute systems, the water content exceeds the solid volume fraction by far, and hence particle interaction is negligible. With increasing ϕ_s, particle distances decrease and percolation occurs. Most cementitious pastes in concrete contain solid volume fractions between ϕ_s = 0.40 and ϕ_s = 0.60. In suspension rheology, they are considered as densely packed systems with high interaction forces that build up a particle network [12]. The rheological parameters i.e. the yield stress τ_0, which is the stress that needs to be surpassed for the start-up of flow, and viscosity η, which is the resistance against flow, depend on the particle network strength and agglomeration as well as de-flocculation gradient in dependence of the shear rate. Thus, cementitious pastes are classified as visco-plastic Bingham- or Herschel-Bulkley fluids (fluids with a yield stress and shear-thinning or shear-thickening behavior).

1.2 Numerical flow simulation using computational fluid dynamics (CFD)

Continuum fluid mechanics describes the spatial change of a quantity within a volume space using the physical constitutive laws of mass conservation and momentum equations and thus is a phenomenological field theory. It is used for the description of stress and deformation [13, 14]. The Navier-Stokes equations are the governing constitutive equations for linear-viscous flow of matter. They consist of the equations for the conservation of mass and conservation of momentum:

$$\nabla \boldsymbol{u} = 0 \tag{1}$$

$$\frac{\partial}{\partial t}(\rho \boldsymbol{u}) + \rho \nabla^2 \boldsymbol{u} = -\nabla p + \nabla \tau + \rho g \tag{2}$$

With $\boldsymbol{u}$ as velocity vector field in [m/s], p as scalar pressure in [Nsm^{-2}] and τ as the viscous stress tensor in [Nsm^{-2}]. Coupled with the equation of state for pressure, temperature and density, they describe viscous flow through a velocity gradient (diffusive viscous term) and a pressure term for Generalized Newtonian Fluids (GNF). Conservation of mass for GNFs is simplified by the assumption of incompressibility ($\partial\rho/\partial t$=0). For non-Newtonian flow, shear stress is described by a rheological model incorporating the strain rate dependent apparent viscosity η in [Pas]. In case of Herschel-Bulkley fluids, the shear stress τ is expressed through

$$\tau(\dot{\gamma}) = \tau_0 + k\dot{\gamma}^n \; for \; \tau > \tau_0 \tag{3}$$
$$\dot{\gamma} = 0 \; for \; \tau \leq \tau_0$$

With τ_0 as yield stress in [Pa], $\dot{\gamma}$ as shear rate in [s^{-1}], k as consistency index and n as Herschel-Bulkley index, characterizing shear-thinning behavior in case of $n < 1$, Bingham flow in case of $= 1$ and shear-thickening flow if $n > 1$. Acc. eq. (3), the shear rate dependent viscosity η calculates as

$$\eta(\dot{\gamma}) = \frac{\tau_0}{\dot{\gamma}} + k\dot{\gamma}^{n-1} \tag{4}$$

No-shear-rate zones cause numerical instabilities. Viscosity approximations for shear rates close to zero are the Papanastasiou approach [15], e.g. applied by Gram in [16], or bi-viscous regularization, described by O'Donovan and Tanner [17] and applied by de Schryver et al in [18]. They prevent singularity in the zero-shear-rate zone and thus mathematical instabilities. CFD programs calculate the physical flow parameters, i.e. velocity gradients and pressure, for each discretized element of a continuum by solving the Navier-Stokes equations for each element. Boundary conditions, cell sizes due to mesh definition, mathematical calculation formulas and the chosen algorithms for pressure-velocity coupling for solving the Navier-Stokes equations affect the numerical results, wherefore a clear benchmark analysis in CFD is crucial for reliable calculation results. For concrete applications, this was analyzed by Haustein et al. in [19].

2 MATERIALS AND METHODS

2.1 Concept of investigation and material mixtures

We present the flow simulation for cementitious pastes with varying non-Newtonian rheological behavior but similar flow during a short flow range: Experimental flow was analyzed through the empirical stoppage tests mini slump flow (see Figure 1 (b)) and mini L-Box test (see Figure 1(c)), as previously presented by the authors in [20]. Equal flowability properties for the flow range of $\dot{\gamma} = 5 - 10\ s^{-1}$ (equaling short flow during a mini slump flow test) were ensured through an adjusted addition of Polycarboxylatether (PCE)-based superplasticizer for a mini slump flow value of 250 mm acc. [8].

Table 1: Cement paste mixtures

Mixture	w/c ratio [-]	Solid volume fraction [-]	Cement [kg/m³]	Water [kg/m³][1]	PCE [% bwoc[2]]	Paste density [kg/m³]
0.45	0.40	0.45	1,399.5	550	0.18	1,950
0.48	0.35	0.48	1,492.8	520	0.60	2,010
0.52	0.30	0.52	1,617.2	480	0.93	2,100
0.55	0.26	0.55	1,710.5	450	1.40	2,160
0.58	0.23	0.58	1,803.8	420	2.05	2,220

[1] The water content of the PCE was subtracted from the water amount to be added

[2] bwoc: by weight of cement

Rheological parameters of several cementitious pastes with solid volume fractions ranging from $\phi_s = 0.45$ to $\phi_s = 0.58$, see Table 1, analyzed using parallel-plate rheometry (see Figure 1(a)), served as computational input parameters. Computational modeling of paste flow was

conducted using the software OpenFOAM and compared to the results of the flow experiments. Ordinary Portland Cement (OPC) CEM I 42.5 N from Heidelberg Cement, Germany, deionized water and PCE-based superplasticizer from BASF, Germany, were used. The water was set to a temperature for a constant paste temperature of 20.0°C. Mixture proportions are presented in Table 1.

2.2 Flow analysis: Rheometry and empirical stoppage tests

All cement pastes were prepared as a batch of 0.5 l. Pastes were mixed for 01:30 min at 1,700 rpm and pre-sheared before the rheometric measurement and empirical stoppage tests for further 30 sec at 1,700 rpm. Rheometric measurements were conducted in an Anton Paar Rheometer using parallel plates with a diameter of 50 mm, a gap height of 1 mm and serrated surfaces (see Figure 1(a)). The shear profile was a decreasing step-rate test with shear rates decreasing from 80 s^{-1} to 0.02 s^{-1}, each step taking 6 sec. Raw data conversion from rotational speed ω [rpm] and torque T [Nm] to shear rate $\dot{\gamma}$ [s^{-1}]and shear stress [Pa] followed the procedure explained by the author e.g. in [21].

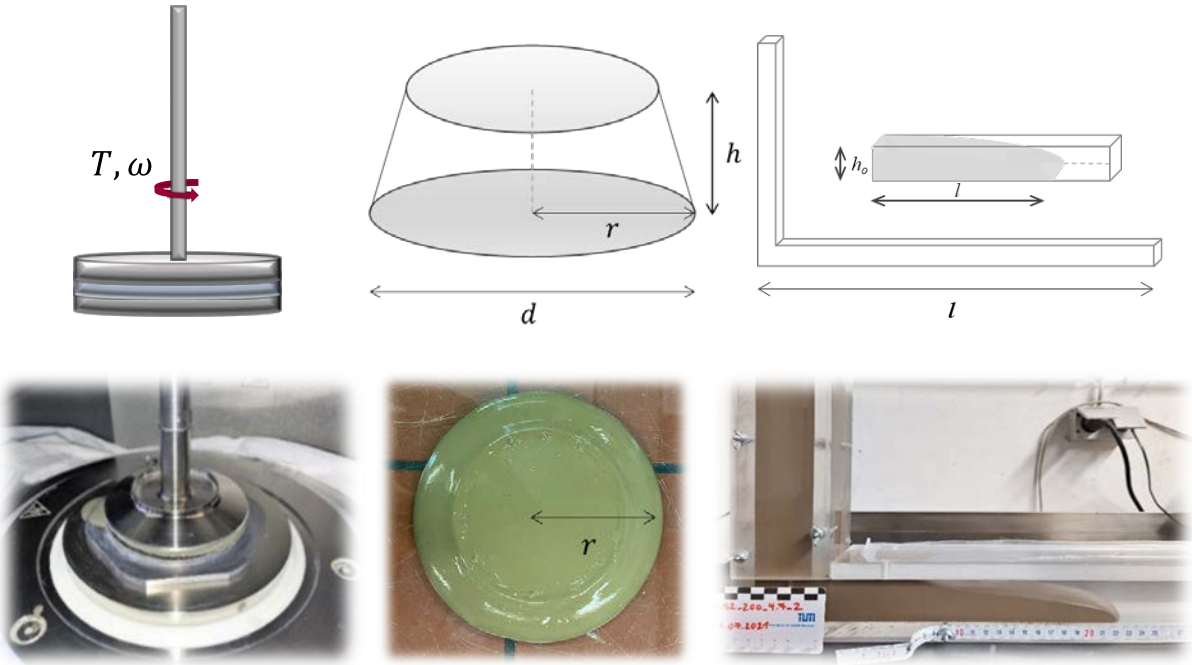

Figure 1 Schematical illustration and experimental figures of flow analysis methods (a) parallel plates rheometry, (b) mini slump flow test and (c) mini L-Box test

Empirical stoppage tests (Mini slump flow, see Figure 1(b) and mini L-Box, see Figure 1(c)) were conducted for the analysis of empirical yield stress and served as validation for the computational flow simulation. Yield stress values for mini slump flow were calculated acc. Roussel et al. [22]:

$$\tau_0 = \frac{225\rho g V^2}{128\pi^2 R^5} \tag{5}$$

Where $\boldsymbol{\varrho}$ is the paste density in [kg/m³], $\boldsymbol{g}$ the specific gravity in [m/s²], $\boldsymbol{V}$as the total sample volume and $\boldsymbol{R}$ is the slump radius. Nguyen et al. calculated the empirical correlation between the final flow length in an L-Box and the yield stress as:

$$L = \frac{h_0}{A} + \frac{l_0}{2A}\ln\left(\frac{l_0}{l_0+2h_0}\right) \quad \text{with } A = \frac{2\tau_0}{\rho g l_0} \tag{6}$$

Where L is the flow length, h_o is the final height of the flow body and $l_o$is the framework depth [23]. Both stoppage tests were conducted for all pastes; a mini L-Box geometry was introduced as already published by the author in [20].

2.3 Computational modeling

Numerical flow simulation was conducted with the open-source software OpenFOAM. OpenFOAM (Open-source Field Operation And Manipulation, https://openfoam.org), which uses the Finite Volume Method (FVM) to solve the partial differential equations of flow. FVM discretizes a continuum spatially through meshing. As FVM is used for single-phase flow, multiphase flow was analyzed through the Volume of Fluids (VoF) method. VoF uses the Eulerian mesh approach and extends single phase to multiphase flow by introducing a weighting quantity α:

$$\frac{\partial \alpha}{\partial t} + \nabla(\alpha \boldsymbol{u}) + \nabla * (\alpha(1-\alpha)\boldsymbol{u}_r) = 0 \tag{7}$$

If $\alpha = 0$, the whole cell is filled with the first phase (generally air). If $\alpha = 1$, the cell is fully filled with the second phase. Herschel-Bulkley modeling in combination with the bi-viscous regularization model was chosen to prevent singularity:

$$\eta = \min\begin{cases}\eta_0 \\ \dfrac{\tau_0}{\dot{\gamma}} + k\dot{\gamma}^{n-1}\end{cases} \tag{8}$$

For the definition of η_0, we followed the proposal by Donovan and Tanner and set $\eta_0 = 1{,}000\eta$ [17]. In OpenFOAM, the pimple solver was used for the pressure-velocity coupling. The discretization scheme was Gauss linear. Slight under-relaxation was chosen to prevent instabilities. The maximum Courant number was set to 0.5. Boundary conditions and computational grid sizes are illustrated in Figure 2 and Table 2. They are based on literature study and benchmarking results using the Herschel-Bulkley fluid Carbopol, similar to the research shown in Schaer et al. in [24].

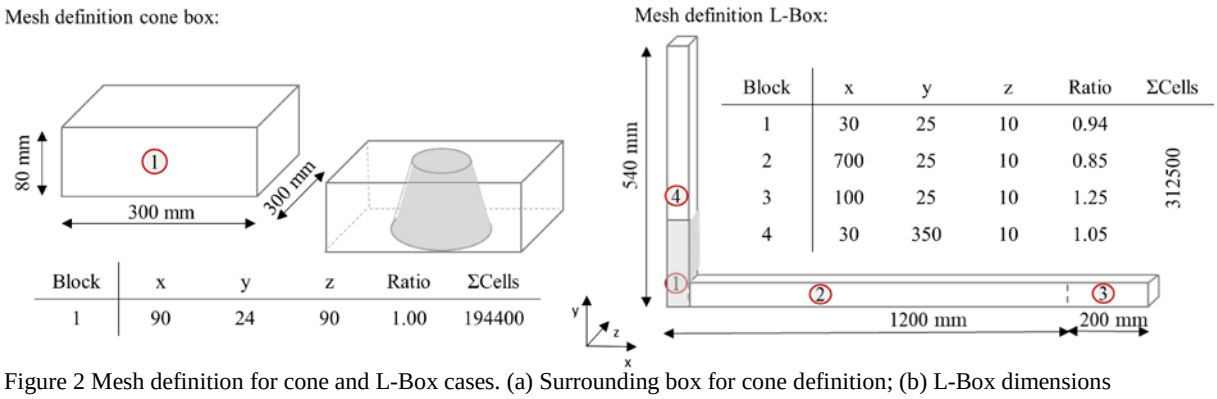

Figure 2 Mesh definition for cone and L-Box cases. (a) Surrounding box for cone definition; (b) L-Box dimensions

For the Cone setup, a three-dimensional box was initialized. Subsequently, the cement paste before lifting the cone at $t = 0$ was implemented by the geometrical definition of α as cone-shaped, as illustrated Figure 2 (a). Figure 2 (b) shows the L-Box geometry with the cement paste stuck in the vertical box before lifting the L-Box gate at $t = 0$.

Table 2: Boundary conditions in OpenFOAM

Face	Field	Cone and L-Box Type	Definition	Value
Atmosphere	U	Neumann	Zero gradient	$\nabla U = 0$
	p	Dirichlet	Zero value	$p = 0$
Walls	U	Dirichlet	No Slip	$U = 0$
	p	Neumann	Zero gradient	$\nabla p = 0$

3 RESULTS AND DISCUSSION

3.1 Rheological flow analysis

Flow curves for all test series are illustrated in Figure 3. The log-log illustration shows the non-Newtonian flow below and beyond critical shear. Below critical shear, agglomeration processes take place especially with increasing solid volume fraction ϕ. At a shear rate of $\dot{\gamma} \sim 10\ s^{-1}$, viscosity appears similar, which corresponds to the apparent shear rate during slump flow and explains similar slump flow values. However, the flow curves show that even in case of similar slump flow values, rheological parameters change in dependence of ϕ (see Table 3).

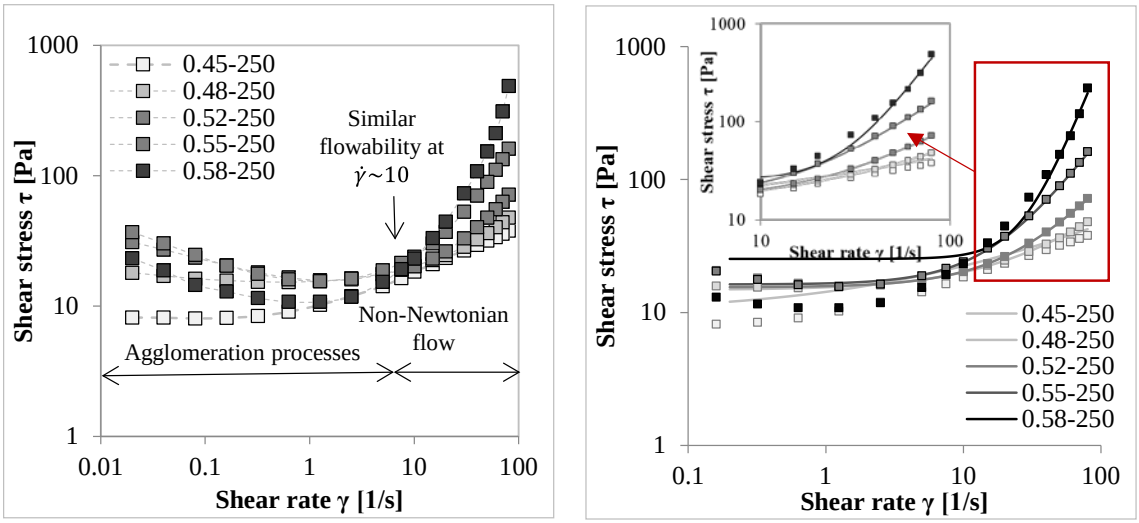

Figure 3 (a) Experimental flow curves for all test series after transversion from raw data to flow data with agglomeration below critical shear and non-Newtonian flow beyond critical shear, (b) Herschel-Bulkley regression for the range beyond the critical shear

Figure 3(b) shows the Herschel-Bulkley regression acc. to eq. (3) for the flow range beyond critical shear. The calculated rheological parameters and the according simulation input parameters for OpenFOAM are given in Table 3. Simulation input parameters are the density dependent kinematic values.

Table 3: Rheological parameters and subsequent numerical input parameters

Test series	Herschel-Bulkley regression				Computational input		
	$\dot{\gamma}_{crit}$	$\tau_{0,H-B}$ (Pa)	k ()	n (-)	$\tau_{0,H-B}$ (m²/s²)	k (m²/s²)	n (-)
CP	-	8.97	3.12	0.43	0.0018	4.4E-03	0.43
0.45	0.08	10.00	4.28	0.46	0.0051	2.2E-03	0.46
0.48	0.63	14.81	0.70	0.88	0.0074	3.5E-04	0.88
0.52	1.25	15.45	0.32	1.18	0.0075	1.5E-04	1.18
0.55	1.25	16.29	0.31	1.40	0.0075	1.4E-04	1.40
0.58	1.25	25.33	0.01	2.59	0.0110	2.2E-06	2.59

The experimental flow test results and the computed yield stress values from the analytical solution (see eq. (5) and (6)) are given in Table 4.

Table 4: Flow parameters from empirical stoppage tests

Test series	Slump flow			L-Box		
	Slump flow (mm)	$\tau_{R,A}$ (Pa)[1]	h_0 (cm)	l_i (mm)	Time of flow (s)	τ_N (Pa)[2]
CP	258	5.8	2.1	504	>100	2.6
0.45	250	13.2	2.4	505	28	6.8
0.48	249	13.9	2.8	465	29	9.8

0.52	251	13.9	3.0	380	42	16.2
0.55	247	15.6	3.6	354	28	20.5
0.58	250	15.0	3.8	326	32	24.9ö

[1] Empirical stoppage test correlation acc. eq. (4)

[2] Empirical stoppage test correlation acc. eq. (5)

The flow divergence between the time-independent slump flow test and time-dependent L-Box flow is illustrated in Figure 4. Whilst the flow length in the slump flow test stays relatively constant with increasing ϕ, the L-Box flow length decreases (see Figure 4(a)). The normalized velocity profile over time is shown for all L-Box tests in Figure 4(b). One can see that with increasing packing density, the cement pastes flows over a longer period until the final flow length is reached. The longer flow time corresponds to lower velocity and thus smaller shear rates during flow. Agglomeration processes that take place at lower shear rates at high packing densities explain the flow loss with increasing packing density.

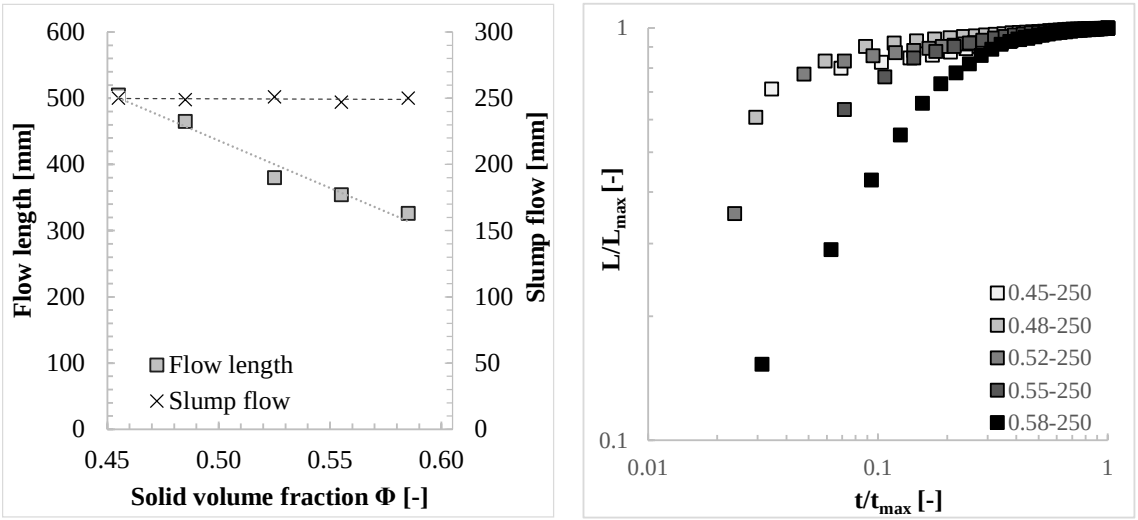

(b)

Figure 4 Flow analysis of L-Box test: (a) Final flow length and slump flow value for all test series, (b) Normalized time-dependent flow distance in the L-Box over time

3.2 Computational flow simulation

Computational flow simulation was conducted for all test series using the rheological input parameters given in Table 3. A schematic illustration of CFD simulation is shown in Figure 5. Flow length results of both set-ups from numerical simulation and normalized flow length with time in the L-Box set-up are shown in Figure 6. Figure 6(a) shows the comparison between experimental and simulation results.

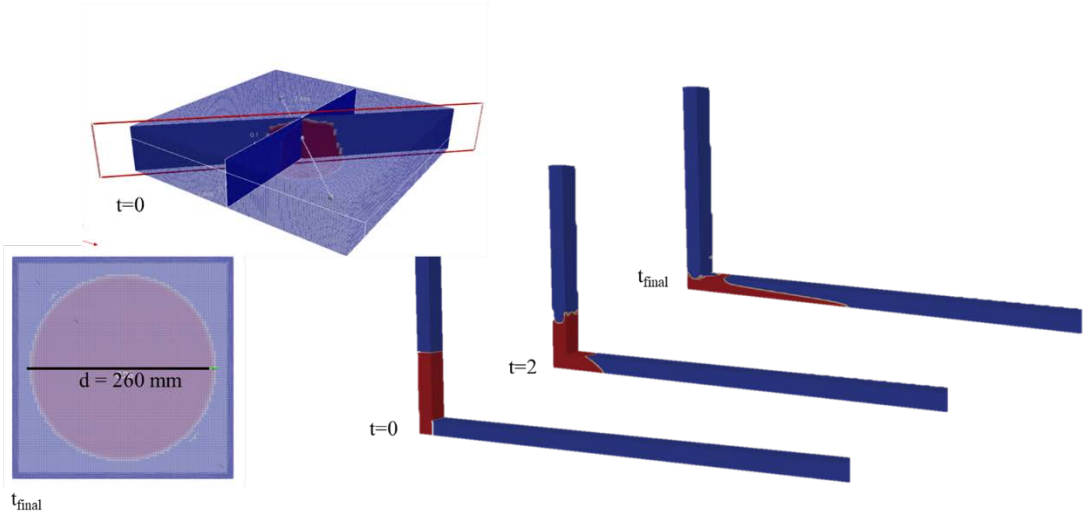

Figure 5 Schematic illustration of flow simulation for slump flow test and L-Box test

Table 5: Simulation results

Test series	Slump flow		L-Box	
	Slump flow (mm)	Time of flow (s)	Flow length (mm)	Time of flow (s)
0.45	280	5.0	576	14.0
0.48	280	6.0	488	10.2
0.52	280	8.5	488	10.5
0.55	276	8.5	487	9.5
0.58	251	10.0	462	11.5

The simulation results slightly overestimate the final slump flow. With increasing solid volume fraction Φ, the numerical slump flow slightly decreases; however, the simulation results do not represent the real decrease in flow loss. Comparison of L-Box experiments and simulation shows that unlike in the experimental results, the numerical L-Box flow length only decreases slightly with increasing Φ. Figure 6(b) shows the flow progress in the L-Box simulations. In comparison to Figure 4(b), the flow between different paste series does not diverge as pronounced in the simulation as in the real flow experiments. This can be explained by the implementation of the Herschel-Bulkley model in CFD simulation, that does not incorporate time-dependent thixotropic or viscoelastic effects at low shear rates and thus does not apply for cementitious pastes at very high packing densities.

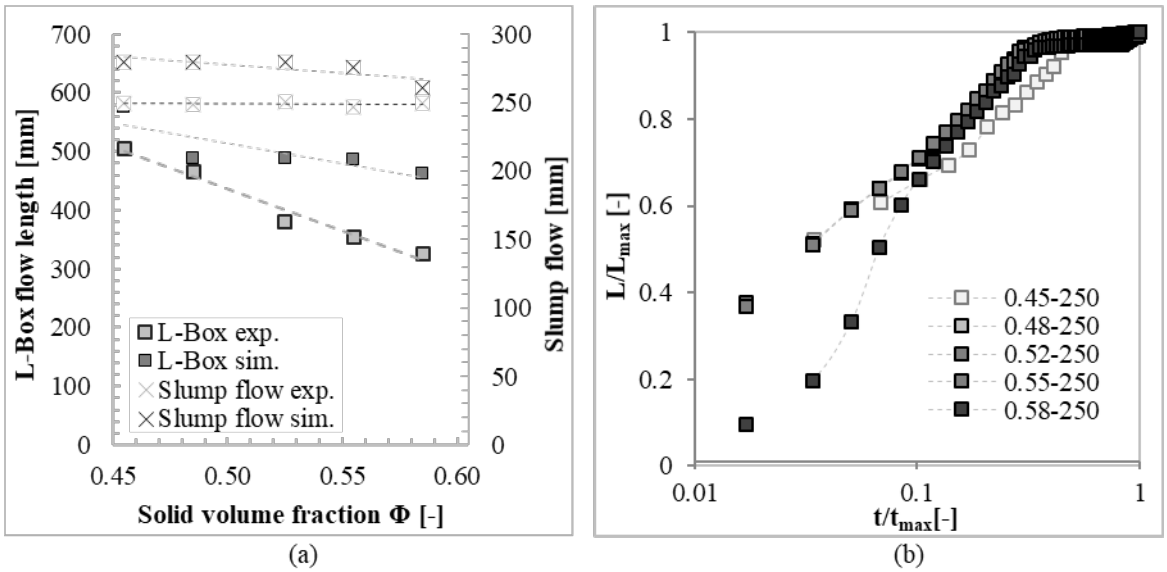

Figure 6 (a) Comparison between experimental and numerical test results for slump flow and L-Box tests of all test series and (b) normalized flow length with time for L-Box test series

3.3 Effect of rheological properties on computational validity

The suitability of the Herschel-Bulkley model depends on the test set-up and thus timescale of flow and the rheological properties of the cement paste mixture: For flow simulation over a short time scale (slump flow analysis), the Herschel-Bulkley model does not cause errors in the flow simulation. With increasing solid volume fraction, the Herschel-Bulkley model does not contain enough information to depict the flow length decrease measured in experimental flow analysis in the time-dependent simulation: With increasing ϕ, particle distances decrease, and thus interparticle forces tend to increase. As soon as the apparent shear rate is too low to break the cementitious network, particles agglomerate, which leads to increasing viscosities. This time- and shear-dependent rheological behavior is not described by the Herschel-Bulkley model, and as a consequence is not captured by the numerical analysis as well. For cementitious pastes with no or low critical shear (see Table 3), the numerical error by Herschel-Bulkley description is low. Thus, the Herschel-Bulkley model is sufficient for flow description beyond a certain critical shear (see Figure 3) and for a clear Herschel-Bulkley fluid, which is the case for solid volume fractions at Φ=0.45 or Φ=0.48. In time-dependent flow analysis with low velocities due to high viscosities and thus low shear rates, agglomeration processes due to low shear rates and thus thixotropy are not taken into account in the flow simulation. This leads to increasing divergence between real flow, where agglomeration takes place, and flow simulation, where flow stops when the shear rate approaches zero. The difference between the shear rate distribution at high and low solid volume fraction pastes is given in Figure 7, where the shear rate distribution of test series 0.48-250 and 0.58-250 are compared directly after the start-up of flow ($t = 2\ sec$) and towards the end of flow ($t = 10\ sec$).

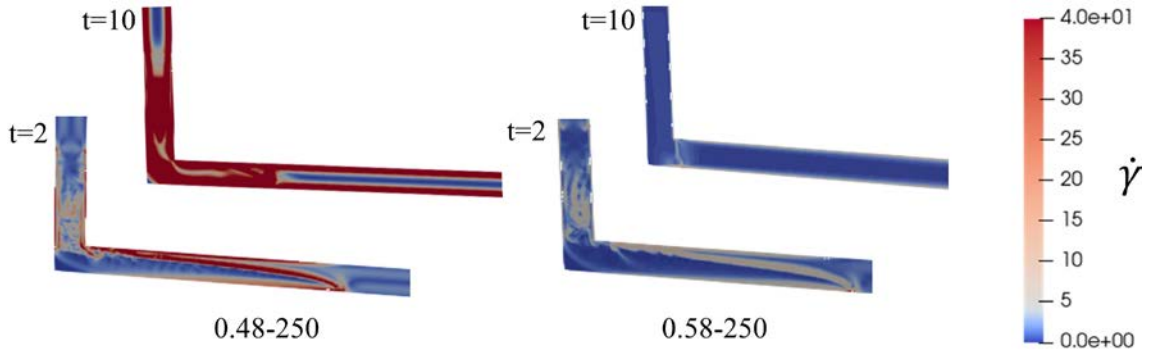

Figure 7 Shear rate distribution for t=2 sec and t=10sec for the test series 0.48-250 and 0.58-250

One can see that shear rates $\dot{\gamma}$ are higher for test series 0.48-250. For test series 0.58-250, the shear rates $\dot{\gamma}$ are very low already at the beginning of flow, and increase over time. As soon as shear rates are below the critical shear $\dot{\gamma}_{crit}$, the rheological behavior is not implemented correctly into the simulation. For correct numerical simulation of cementitious pastes with high solid volume fraction, agglomeration processes have to be taken into account.

4 CONCLUSION

Numerical flow simulation of cementitious building materials gives us the chance to analyze and predict flowability without the need of time-consuming laboratory experiments. The usability of CFD analysis for Bingham- and Herschel-Bulkley materials is already state-of-the-art and could be implemented successfully. With increasing rheological complexity, i.e. non-Newtonian behavior, agglomeration processes (thixotropy) at low shear rates and slow flow due to high viscosities, it was found that other than Herschel-Bulkley models need to be implemented for precise numerical simulations. If flow processes take place over a longer period with successively decreasing shear rates, time- and shear-dependent changes in material rheology need to be implemented into numerical rheological models. Further, a clear analysis of boundary conditions for non-Newtonian cementitious pastes is still lacking. This is part of ongoing research.

REFERENCES

[1] ROUSSEL, N. ; BESSAIES-BEY, H. ; KAWASHIMA, S. ; MARCHON, D. ; VASILIC, K. ; WOLFS, R.: *Recent advances on yield stress and elasticity of fresh cement-based materials*. In: *Cement and Concrete Research* 124 (2019), S. 105798

[2] Ferzinger, J.H.; Peric, M.: *Numerische Strömungsmechanik*. Berlin, Heidelberg : Springer Berlin Heidelberg, 2008, ISBN: 978-3-540-67586-0

[3] FARINA, Angiolo ; FUSI, Lorenzo ; MIKELIĆ, Andro ; SACCOMANDI, Giuseppe ; SEQUEIRA, Adélia ; TORO, Eleuterio F. ; ROSSO, Fabio: *Non-Newtonian Fluid Mechanics and Complex Flows*. Cham : Springer International Publishing, 2018

[4] ROUSSEL, Nicolas ; GRAM, Annika ; ET AL: *Numerical simulations of concrete flow : A benchmark comparison*. In: *Cement and Concrete Research* 79 (2016), S. 265–271

[5] WALLEVIK, Jon Elvar: *Rheological properties of cement paste : Thixotropic behavior and structural breakdown*. In: *Cement and Concrete Research* 39 (2009), Nr. 1, S. 14–29

[6] ROUSSEL, N. ; CUSSIGH, F.: *Distinct-layer casting of SCC: The mechanical consequences of thixotropy*. In: *Cement and Concrete Research* 38 (2008), Nr. 5, S. 624–632

[7] SCHRYVER, Robin de ; SCHUTTER, Geert de: *Insights in thixotropic concrete pumping by a Poiseuille flow extension*. In: *Applied Rheology* 30 (2020), Nr. 1, S. 77–101

[8] *DIN EN 12350-8:2019-09, Prüfung von Frischbeton - Teil_8: Selbstverdichtender Beton- Setzfließversuch*

[9] NORMENAUSSCHUSS BAUWESEN: *DIN EN 12350-10: Prüfung von Frischbeton - Teil 10: Selbstverdichtender Beton - L-Kasten-Versuch* (2010)

[10] LOWKE, Dirk: *Sedimentationsverhalten und Robustheit Selbstverdichtender Betone* : *Optimierung auf Basis der Modellierung der interpartikulären Wechselwirkungen in zementbasierten Suspensionen*. Technische Universität München, Dissertation. 2013

[11] FLATT, Robert J. ; BOWEN, Paul ; HOUST, Y. F. ; HOFMANN, H.: Modelling interparticle forces and yield stress of cement suspensions. In: *Proceedings of the 11th International Congress on the Chemistry of Cement (ICCC)* : *Cement's Contribution to Development in the 21st Century* : Document Transformation Technologies, 2003, S. 618–627

[12] GENOVESE, Diego B.: *Shear rheology of hard-sphere, dispersed, and aggregated suspensions, and filler-matrix composites*. In: *Advances in colloid and interface science* 171-172 (2012), S. 1–16

[13] ALTENBACH, Holm: *Kontinuumsmechanik*. Berlin, Heidelberg : Springer Berlin Heidelberg, 2018

[14] RÜTTEN, Markus: *Verallgemeinerte newtonsche Fluide*. Berlin, Heidelberg : Springer Berlin Heidelberg, 2019

[15] PAPANASTASIOU, Tasos C.: *Flows of Materials with Yield*. In: *Journal of Rheology* 31 (1987), Nr. 5, S. 385–404

[16] GRAM, Annika: *Modelling Bingham Suspensional Flow* : *Influence of Viscosity and Particle Properties Applicable to Cementitious Materials*. Stockholm. Dissertation. 2015

[17] O'DONOVAN, E. J. ; TANNER, R. I.: *Numerical study of the Bingham squeeze film problem*. In: *Journal of Non-Newtonian Fluid Mechanics* 15 (1984), Nr. 1, S. 75–83

[18] SCHRYVER, Robin de ; EL CHEIKH, Khadija ; LESAGE, Karel ; YARDIMCI, Mert Yücel ; SCHUTTER, Geert de: *Numerical Reliability Study Based on Rheological Input for Bingham Paste Pumping Using a Finite Volume Approach in OpenFOAM*. In: *Materials (Basel, Switzerland)* 14 (2021), Nr. 17

[19] HAUSTEIN, M. A. ; ESLAMI PIRHARATI, M. ; FATAEI, S. ; IVANOV, D. ; JARA HEREDIA, D. ; KIJANSKI, N. ; LOWKE, D. ; MECHTCHERINE, V. ; ROSTAN, D. ; SCHÄFER, T. ; SCHILDE, C. ; STEEB, H. ; SCHWARZE, R.: *Benchmark Simulations of Dense Suspensions Flow Using Computational Fluid Dynamics*. In: *Frontiers in Materials* 9 (2022)

[20] THIEDEITZ, Mareike ; HABIB, Nasime ; KRÄNKEL, Thomas ; GEHLEN, Christoph: *L-Box Form Filling of Thixotropic Cementitious Paste and Mortar*. In: *Materials (Basel, Switzerland)* 13 (2020), Nr. 7

[21] THIEDEITZ, Mareike ; DRESSLER, Inka ; KRÄNKEL, Thomas ; GEHLEN, Christoph ; LOWKE, Dirk: *Effect of Pre-Shear on Agglomeration and Rheological Parameters of Cement Paste*. In: *Materials (Basel, Switzerland)* 13 (2020), Nr. 9

[22] ROUSSEL, N. ; STEFANI, C. ; LEROY, R.: *From mini-cone test to Abrams cone test* : *Measurement of cement-based materials yield stress using slump tests*. In: *Cement and Concrete Research* 35 (2005), Nr. 5, S. 817–822

[23] NGUYEN, T.L.H. ; ROUSSEL, N. ; COUSSOT, P.: *Correlation between L-box test and rheological parameters of a homogeneous yield stress fluid*. In: *Cement and Concrete Research* 36 (2006), Nr. 10, S. 1789–1796

[24] N SCHAER, J. VAZQUEZ, M. DUFRESNE, G ISENMANN, J. WERTEL: *On the Determination of the Yield Surface within the Flow of Yield Stress Fluids using Computational Fluid Dynamics*. In: *Journal of Applied Fluid Mechanics* 11 (2018), Nr. 4, S. 971–982